

# Charged Particle Cross Sections in Photoproduction and Extraction of the Gluon Density in the Photon

H1 Collaboration

## Abstract

Photoproduction data collected with the H1 detector at HERA in 1994 are used to study the cross-sections for inclusive charged particle production and the structure of the photon. The differential cross-sections  $d\sigma/dp_T^2$ , for  $|\eta| < 1$  in the HERA laboratory frame, and  $d\sigma/d\eta$  for  $p_T > 2$  GeV/c and  $p_T > 3$  GeV/c have been measured. Model calculations of these cross-sections, based on perturbative QCD, indicate that the results are sensitive to the parton densities of the photon as well as to higher order effects, which are phenomenologically treated by multiple interactions. This sensitivity is exploited to determine the leading order  $x_\gamma$  distribution of partons in the photon using a new method based on high  $p_T$  charged particles. The gluon content of the photon is extracted and found to rise with decreasing  $x_\gamma$ .

Submitted to Eur. Phys. J.

# H1 Collaboration

C. Adloff<sup>34</sup>, M. Anderson<sup>22</sup>, V. Andreev<sup>25</sup>, B. Andrieu<sup>28</sup>, V. Arkadov<sup>35</sup>, C. Arndt<sup>11</sup>,  
I. Ayyaz<sup>29</sup>, A. Babaev<sup>24</sup>, J. Bähr<sup>35</sup>, J. Bán<sup>17</sup>, P. Baranov<sup>25</sup>, E. Barrelet<sup>29</sup>, W. Bartel<sup>11</sup>,  
U. Bassler<sup>29</sup>, P. Bate<sup>22</sup>, M. Beck<sup>13</sup>, A. Beglarian<sup>11,40</sup>, O. Behnke<sup>11</sup>, H.-J. Behrend<sup>11</sup>,  
C. Beier<sup>15</sup>, A. Belousov<sup>25</sup>, Ch. Berger<sup>1</sup>, G. Bernardi<sup>29</sup>, G. Bertrand-Coremans<sup>4</sup>, P. Biddulph<sup>22</sup>,  
J.C. Bizot<sup>27</sup>, V. Boudry<sup>28</sup>, W. Braunschweig<sup>1</sup>, V. Brisson<sup>27</sup>, D.P. Brown<sup>22</sup>, W. Brückner<sup>13</sup>,  
P. Bruel<sup>28</sup>, D. Bruncko<sup>17</sup>, J. Bürger<sup>11</sup>, F.W. Büsler<sup>12</sup>, A. Buniatian<sup>32</sup>, S. Burke<sup>18</sup>,  
G. Buschhorn<sup>26</sup>, D. Calvet<sup>23</sup>, A.J. Campbell<sup>11</sup>, T. Carli<sup>26</sup>, E. Chabert<sup>23</sup>, M. Charlet<sup>4</sup>,  
D. Clarke<sup>5</sup>, B. Clerbaux<sup>4</sup>, S. Cocks<sup>19</sup>, J.G. Contreras<sup>8,42</sup>, C. Cormack<sup>19</sup>, J.A. Coughlan<sup>5</sup>,  
M.-C. Cousinou<sup>23</sup>, B.E. Cox<sup>22</sup>, G. Cozzika<sup>10</sup>, J. Cvach<sup>30</sup>, J.B. Dainton<sup>19</sup>, W.D. Dau<sup>16</sup>,  
K. Daum<sup>39</sup>, M. David<sup>10</sup>, M. Davidsson<sup>21</sup>, A. De Roeck<sup>11</sup>, E.A. De Wolf<sup>4</sup>, B. Delcourt<sup>27</sup>,  
R. Demirchyan<sup>11,40</sup>, C. Diaconu<sup>23</sup>, M. Dirkmann<sup>8</sup>, P. Dixon<sup>20</sup>, W. Dlugosz<sup>7</sup>, K.T. Donovan<sup>20</sup>,  
J.D. Dowell<sup>3</sup>, A. Droutskoi<sup>24</sup>, J. Ebert<sup>34</sup>, G. Eckerlin<sup>11</sup>, D. Eckstein<sup>35</sup>, V. Efremenko<sup>24</sup>,  
S. Egli<sup>37</sup>, R. Eichler<sup>36</sup>, F. Eisele<sup>14</sup>, E. Eisenhandler<sup>20</sup>, E. Elsen<sup>11</sup>, M. Enzenberger<sup>26</sup>,  
M. Erdmann<sup>14</sup>, A.B. Fahr<sup>12</sup>, L. Favart<sup>4</sup>, A. Fedotov<sup>24</sup>, R. Felst<sup>11</sup>, J. Feltesse<sup>10</sup>, J. Ferencei<sup>17</sup>,  
F. Ferrarotto<sup>32</sup>, M. Fleischer<sup>8</sup>, G. Flügge<sup>2</sup>, A. Fomenko<sup>25</sup>, J. Formánek<sup>31</sup>, J.M. Foster<sup>22</sup>,  
G. Franke<sup>11</sup>, E. Gabathuler<sup>19</sup>, K. Gabathuler<sup>33</sup>, F. Gaede<sup>26</sup>, J. Garvey<sup>3</sup>, J. Gayler<sup>11</sup>,  
R. Gerhards<sup>11</sup>, S. Ghazaryan<sup>11,40</sup>, A. Glazov<sup>35</sup>, L. Goerlich<sup>6</sup>, N. Gogitidze<sup>25</sup>, M. Goldberg<sup>29</sup>,  
I. Gorelov<sup>24</sup>, C. Grab<sup>36</sup>, H. Grässler<sup>2</sup>, T. Greenshaw<sup>19</sup>, R.K. Griffiths<sup>20</sup>, G. Grindhammer<sup>26</sup>,  
T. Hadig<sup>1</sup>, D. Haidt<sup>11</sup>, L. Hajduk<sup>6</sup>, T. Haller<sup>13</sup>, M. Hampel<sup>1</sup>, V. Haustein<sup>34</sup>, W.J. Haynes<sup>5</sup>,  
B. Heinemann<sup>11</sup>, G. Heinzelmann<sup>12</sup>, R.C.W. Henderson<sup>18</sup>, S. Hengstmann<sup>37</sup>, H. Henschel<sup>35</sup>,  
R. Heremans<sup>4</sup>, I. Herynek<sup>30</sup>, K. Hewitt<sup>3</sup>, K.H. Hiller<sup>35</sup>, C.D. Hilton<sup>22</sup>, J. Hladký<sup>30</sup>,  
D. Hoffmann<sup>11</sup>, T. Holtom<sup>19</sup>, W. Hoprich<sup>13</sup>, R. Horisberger<sup>33</sup>, V.L. Hudgson<sup>3</sup>, S. Hurling<sup>11</sup>,  
M. Ibbotson<sup>22</sup>, Ç. İssever<sup>8</sup>, H. Itterbeck<sup>1</sup>, M. Jacquet<sup>27</sup>, M. Jaffre<sup>27</sup>, D.M. Jansen<sup>13</sup>,  
L. Jönsson<sup>21</sup>, D.P. Johnson<sup>4</sup>, H. Jung<sup>21</sup>, H.K. Kästli<sup>36</sup>, M. Kander<sup>11</sup>, D. Kant<sup>20</sup>,  
M. Kapichine<sup>9</sup>, M. Karlsson<sup>21</sup>, O. Karschnik<sup>12</sup>, J. Katzy<sup>11</sup>, O. Kaufmann<sup>14</sup>, M. Kausch<sup>11</sup>,  
I.R. Kenyon<sup>3</sup>, S. Kermiche<sup>23</sup>, C. Keuker<sup>1</sup>, C. Kiesling<sup>26</sup>, M. Klein<sup>35</sup>, C. Kleinwort<sup>11</sup>,  
G. Knies<sup>11</sup>, J.H. Köhne<sup>26</sup>, H. Kolanoski<sup>38</sup>, S.D. Kolya<sup>22</sup>, V. Korbel<sup>11</sup>, P. Kostka<sup>35</sup>,  
S.K. Kotelnikov<sup>25</sup>, T. Krämerkämper<sup>8</sup>, M.W. Krasny<sup>29</sup>, H. Krehbiel<sup>11</sup>, D. Krücker<sup>26</sup>,  
K. Krüger<sup>11</sup>, A. Küpper<sup>34</sup>, H. Küster<sup>2</sup>, M. Kühlen<sup>26</sup>, T. Kurča<sup>35</sup>, B. Laforge<sup>10</sup>, R. Lahmann<sup>11</sup>,  
M.P.J. Landon<sup>20</sup>, W. Lange<sup>35</sup>, U. Langenegger<sup>36</sup>, A. Lebedev<sup>25</sup>, F. Lehner<sup>11</sup>, V. Lemaitre<sup>11</sup>,  
V. Lendermann<sup>8</sup>, S. Levonian<sup>11</sup>, M. Lindstroem<sup>21</sup>, B. List<sup>11</sup>, G. Lobo<sup>27</sup>, E. Lobodzinska<sup>6,41</sup>,  
V. Lubimov<sup>24</sup>, D. Lüke<sup>8,11</sup>, L. Lytkin<sup>13</sup>, N. Magnussen<sup>34</sup>, H. Mahlke-Krüger<sup>11</sup>, E. Malinovski<sup>25</sup>,  
R. Maračec<sup>17</sup>, P. Marage<sup>4</sup>, J. Marks<sup>14</sup>, R. Marshall<sup>22</sup>, G. Martin<sup>12</sup>, H.-U. Martyn<sup>1</sup>,  
J. Martyniak<sup>6</sup>, S.J. Maxfield<sup>19</sup>, S.J. McMahon<sup>19</sup>, T.R. McMahon<sup>19</sup>, A. Mehta<sup>5</sup>, K. Meier<sup>15</sup>,  
P. Merkel<sup>11</sup>, F. Metlica<sup>13</sup>, A. Meyer<sup>11</sup>, A. Meyer<sup>12</sup>, H. Meyer<sup>34</sup>, J. Meyer<sup>11</sup>, P.-O. Meyer<sup>2</sup>,  
S. Mikocki<sup>6</sup>, D. Milstead<sup>11</sup>, J. Moeck<sup>26</sup>, R. Mohr<sup>26</sup>, S. Mohrdieck<sup>12</sup>, F. Moreau<sup>28</sup>, J.V. Morris<sup>5</sup>,  
D. Müller<sup>37</sup>, K. Müller<sup>11</sup>, P. Murín<sup>17</sup>, V. Nagovizin<sup>24</sup>, B. Naroska<sup>12</sup>, Th. Naumann<sup>35</sup>,  
I. Négri<sup>23</sup>, P.R. Newman<sup>3</sup>, H.K. Nguyen<sup>29</sup>, T.C. Nicholls<sup>11</sup>, F. Niebergall<sup>12</sup>, C. Niebuhr<sup>11</sup>,  
Ch. Niedzballa<sup>1</sup>, H. Niggli<sup>36</sup>, D. Nikitin<sup>9</sup>, O. Nix<sup>15</sup>, G. Nowak<sup>6</sup>, T. Nunnemann<sup>13</sup>,  
H. Oberlack<sup>26</sup>, J.E. Olsson<sup>11</sup>, D. Ozerov<sup>24</sup>, P. Palmen<sup>2</sup>, V. Panassik<sup>9</sup>, C. Pascaud<sup>27</sup>,  
S. Passaggio<sup>36</sup>, G.D. Patel<sup>19</sup>, H. Pawletta<sup>2</sup>, E. Perez<sup>10</sup>, J.P. Phillips<sup>19</sup>, A. Pieuchot<sup>11</sup>,  
D. Pitzl<sup>36</sup>, R. Pöschl<sup>8</sup>, G. Pope<sup>7</sup>, B. Povh<sup>13</sup>, K. Rabbertz<sup>1</sup>, J. Rauschenberger<sup>12</sup>, P. Reimer<sup>30</sup>,  
B. Reisert<sup>26</sup>, H. Rick<sup>11</sup>, S. Riess<sup>12</sup>, E. Rizvi<sup>11</sup>, P. Robmann<sup>37</sup>, R. Roosen<sup>4</sup>, K. Rosenbauer<sup>1</sup>,  
A. Rostovtsev<sup>24,12</sup>, F. Rouse<sup>7</sup>, C. Royon<sup>10</sup>, S. Rusakov<sup>25</sup>, K. Rybicki<sup>6</sup>, D.P.C. Sankey<sup>5</sup>,  
P. Schacht<sup>26</sup>, J. Scheins<sup>1</sup>, S. Schleich<sup>15</sup>, P. Schleper<sup>14</sup>, D. Schmidt<sup>34</sup>, D. Schmidt<sup>11</sup>,  
L. Schoeffel<sup>10</sup>, V. Schröder<sup>11</sup>, H.-C. Schultz-Coulon<sup>11</sup>, B. Schwab<sup>14</sup>, F. Sefkow<sup>37</sup>, A. Semenov<sup>24</sup>,  
V. Shekelyan<sup>26</sup>, I. Sheviakov<sup>25</sup>, L.N. Shtarkov<sup>25</sup>, G. Siegmon<sup>16</sup>, Y. Sirois<sup>28</sup>, T. Sloan<sup>18</sup>,  
P. Smirnov<sup>25</sup>, M. Smith<sup>19</sup>, V. Solochenko<sup>24</sup>, Y. Soloviev<sup>25</sup>, V. Spaskov<sup>9</sup>, A. Specka<sup>28</sup>,  
J. Spiekermann<sup>8</sup>, H. Spitzer<sup>12</sup>, F. Squinabol<sup>27</sup>, P. Steffen<sup>11</sup>, R. Steinberg<sup>2</sup>, J. Steinhart<sup>12</sup>,  
B. Stella<sup>32</sup>, A. Stellberger<sup>15</sup>, J. Stiewe<sup>15</sup>, U. Straumann<sup>14</sup>, W. Struczinski<sup>2</sup>, J.P. Sutton<sup>3</sup>,

M. Swart<sup>15</sup>, S. Tapprogge<sup>15</sup>, M. Taševský<sup>30</sup>, V. Tchernyshov<sup>24</sup>, S. Tchetchelnitski<sup>24</sup>,  
 J. Theissen<sup>2</sup>, G. Thompson<sup>20</sup>, P.D. Thompson<sup>3</sup>, N. Tobien<sup>11</sup>, R. Todenhagen<sup>13</sup>, P. Truöl<sup>37</sup>,  
 G. Tsipolitis<sup>36</sup>, J. Turnau<sup>6</sup>, E. Tzamariudaki<sup>11</sup>, S. Udluft<sup>26</sup>, A. Usik<sup>25</sup>, S. Valkár<sup>31</sup>,  
 A. Valkárová<sup>31</sup>, C. Vallée<sup>23</sup>, P. Van Esch<sup>4</sup>, A. Van Haecke<sup>10</sup>, P. Van Mechelen<sup>4</sup>, Y. Vazdik<sup>25</sup>,  
 G. Villet<sup>10</sup>, K. Wacker<sup>8</sup>, R. Wallny<sup>14</sup>, T. Walter<sup>37</sup>, B. Waugh<sup>22</sup>, G. Weber<sup>12</sup>, M. Weber<sup>15</sup>,  
 D. Wegener<sup>8</sup>, A. Wegner<sup>26</sup>, T. Wengler<sup>14</sup>, M. Werner<sup>14</sup>, L.R. West<sup>3</sup>, S. Wiesand<sup>34</sup>,  
 T. Wilksen<sup>11</sup>, S. Willard<sup>7</sup>, M. Winde<sup>35</sup>, G.-G. Winter<sup>11</sup>, C. Wittek<sup>12</sup>, E. Wittmann<sup>13</sup>,  
 M. Wobisch<sup>2</sup>, H. Wollatz<sup>11</sup>, E. Wünsch<sup>11</sup>, J. Žáček<sup>31</sup>, J. Zálešák<sup>31</sup>, Z. Zhang<sup>27</sup>, A. Zhokin<sup>24</sup>,  
 P. Zini<sup>29</sup>, F. Zomer<sup>27</sup>, J. Zsembery<sup>10</sup> and M. zurNedden<sup>37</sup>

- <sup>1</sup> *I. Physikalisches Institut der RWTH, Aachen, Germany<sup>f</sup>*  
<sup>2</sup> *III. Physikalisches Institut der RWTH, Aachen, Germany<sup>f</sup>*  
<sup>3</sup> *School of Physics and Space Research, University of Birmingham, Birmingham, UK<sup>b</sup>*  
<sup>4</sup> *Inter-University Institute for High Energies ULB-VUB, Brussels; Universitaire Instelling Antwerpen, Wilrijk; Belgium<sup>c</sup>*  
<sup>5</sup> *Rutherford Appleton Laboratory, Chilton, Didcot, UK<sup>b</sup>*  
<sup>6</sup> *Institute for Nuclear Physics, Cracow, Poland<sup>d</sup>*  
<sup>7</sup> *Physics Department and IIRPA, University of California, Davis, California, USA<sup>e</sup>*  
<sup>8</sup> *Institut für Physik, Universität Dortmund, Dortmund, Germany<sup>f</sup>*  
<sup>9</sup> *Joint Institute for Nuclear Research, Dubna, Russia*  
<sup>10</sup> *DSM/DAPNIA, CEA/Saclay, Gif-sur-Yvette, France*  
<sup>11</sup> *DESY, Hamburg, Germany<sup>f</sup>*  
<sup>12</sup> *II. Institut für Experimentalphysik, Universität Hamburg, Hamburg, Germany<sup>f</sup>*  
<sup>13</sup> *Max-Planck-Institut für Kernphysik, Heidelberg, Germany<sup>f</sup>*  
<sup>14</sup> *Physikalisches Institut, Universität Heidelberg, Heidelberg, Germany<sup>f</sup>*  
<sup>15</sup> *Institut für Hochenergiephysik, Universität Heidelberg, Heidelberg, Germany<sup>f</sup>*  
<sup>16</sup> *Institut für experimentelle und angewandte Physik, Universität Kiel, Kiel, Germany<sup>f</sup>*  
<sup>17</sup> *Institute of Experimental Physics, Slovak Academy of Sciences, Košice, Slovak Republic<sup>f,j</sup>*  
<sup>18</sup> *School of Physics and Chemistry, University of Lancaster, Lancaster, UK<sup>b</sup>*  
<sup>19</sup> *Department of Physics, University of Liverpool, Liverpool, UK<sup>b</sup>*  
<sup>20</sup> *Queen Mary and Westfield College, London, UK<sup>b</sup>*  
<sup>21</sup> *Physics Department, University of Lund, Lund, Sweden<sup>g</sup>*  
<sup>22</sup> *Department of Physics and Astronomy, University of Manchester, Manchester, UK<sup>b</sup>*  
<sup>23</sup> *CPPM, Université d'Aix-Marseille II, IN2P3-CNRS, Marseille, France*  
<sup>24</sup> *Institute for Theoretical and Experimental Physics, Moscow, Russia*  
<sup>25</sup> *Lebedev Physical Institute, Moscow, Russia<sup>f,k</sup>*  
<sup>26</sup> *Max-Planck-Institut für Physik, München, Germany<sup>f</sup>*  
<sup>27</sup> *LAL, Université de Paris-Sud, IN2P3-CNRS, Orsay, France*  
<sup>28</sup> *LPNHE, École Polytechnique, IN2P3-CNRS, Palaiseau, France*  
<sup>29</sup> *LPNHE, Universités Paris VI and VII, IN2P3-CNRS, Paris, France*  
<sup>30</sup> *Institute of Physics, Academy of Sciences of the Czech Republic, Praha, Czech Republic<sup>f,h</sup>*  
<sup>31</sup> *Nuclear Center, Charles University, Praha, Czech Republic<sup>f,h</sup>*  
<sup>32</sup> *INFN Roma 1 and Dipartimento di Fisica, Università Roma 3, Roma, Italy*  
<sup>33</sup> *Paul Scherrer Institut, Villigen, Switzerland*  
<sup>34</sup> *Fachbereich Physik, Bergische Universität Gesamthochschule Wuppertal, Wuppertal, Germany<sup>f</sup>*  
<sup>35</sup> *DESY, Institut für Hochenergiephysik, Zeuthen, Germany<sup>f</sup>*  
<sup>36</sup> *Institut für Teilchenphysik, ETH, Zürich, Switzerland<sup>i</sup>*  
<sup>37</sup> *Physik-Institut der Universität Zürich, Zürich, Switzerland<sup>i</sup>*  
<sup>38</sup> *Institut für Physik, Humboldt-Universität, Berlin, Germany<sup>f</sup>*  
<sup>39</sup> *Rechenzentrum, Bergische Universität Gesamthochschule Wuppertal, Wuppertal, Germany<sup>f</sup>*  
<sup>40</sup> *Vistor from Yerevan Physics Institute, Armenia*

<sup>41</sup> *Foundation for Polish Science fellow*

<sup>42</sup> *Dept. Fís. Ap. CINVESTAV, Mérida, Yucatán, México*

<sup>a</sup> *Supported by the Bundesministerium für Bildung, Wissenschaft, Forschung und Technologie, FRG, under contract numbers 7AC17P, 7AC47P, 7DO55P, 7HH17I, 7HH27P, 7HD17P, 7HD27P, 7KI17I, 6MP17I and 7WT87P*

<sup>b</sup> *Supported by the UK Particle Physics and Astronomy Research Council, and formerly by the UK Science and Engineering Research Council*

<sup>c</sup> *Supported by FNRS-FWO, IISN-IKW*

<sup>d</sup> *Partially supported by the Polish State Committee for Scientific Research, grant no. 115/E-343/SPUB/P03/002/97 and grant no. 2P03B 055 13*

<sup>e</sup> *Supported in part by US DOE grant DE F603 91ER40674*

<sup>f</sup> *Supported by the Deutsche Forschungsgemeinschaft*

<sup>g</sup> *Supported by the Swedish Natural Science Research Council*

<sup>h</sup> *Supported by GA ČR grant no. 202/96/0214, GA AV ČR grant no. A1010821 and GA UK grant no. 177*

<sup>i</sup> *Supported by the Swiss National Science Foundation*

<sup>j</sup> *Supported by VEGA SR grant no. 2/5167/98*

<sup>k</sup> *Supported by Russian Foundation for Basic Research grant no. 96-02-00019*

# 1 Introduction

The observation that the photon has a hadronic structure was first made more than 30 years ago when the cross-sections of hadronic photoproduction interactions were demonstrated to have dependences on energy and momentum transfer which were similar to those in hadron-hadron interactions [1]. With the advent of the quark-parton model, and subsequently QCD, more quantitative predictions for this hadronic structure became available, and its gross features were identified experimentally in  $e^+e^-$  interactions [2]. Subsequently these features were also observed in hard photoproduction processes [3-15].

Measurements of the photon structure functions in  $e^+e^-$  interactions are directly sensitive to the quark structure of the photon. Only through QCD evolution studies can information be extracted concerning the gluon component of this structure, but the presently available data have not been precise enough for such an analysis. Recently, studies of jets and high  $p_T$  charged particles in photoproduction events at the  $ep$  collider HERA have shown sensitivity to the partonic content of the photon. Here the photon structure is probed by the partons of the proton, rather than by a virtual photon as in  $e\gamma$  collisions. Hence these data are sensitive to both the quark and gluon content of the photon. Leading Order (LO) diagrams are shown in Fig. 1, for so called direct (Fig. 1a; the photon couples directly to the partons in the proton) and resolved (Fig. 1b; the partons of the hadronic component of the photon scatter on the partons of the proton) processes in photoproduction. In LO QCD only the latter process contains information on the partonic structure of the photon.

In [5] inclusive charged particle production has been studied. It was established that the data, in particular the tail at large transverse momentum,  $p_T$ , can be described by Next-to-Leading Order (NLO) QCD calculations. The charged particle distributions as a function of the pseudorapidity<sup>1</sup>,  $\eta = -\ln \tan(\theta/2)$ , were found to be sensitive to the partonic structure of the photon. In this paper we present differential cross-sections  $d\sigma/dp_T^2$  for  $|\eta| < 1$  in the HERA laboratory system, and  $d\sigma/d\eta$  for  $p_T > 2$  GeV/c and  $p_T > 3$  GeV/c for charged particles, measured with the H1 detector. Photoproduction events have been selected by tagging the scattered electron. The data are based on an event sample which is 50 times larger than the one used in [5].

In [6] a first measurement of the gluon content of the photon was presented, while in [8] an effective parton density for the photon was extracted. In this paper the distribution of the momentum fraction  $x_\gamma = E_{parton}/E_\gamma$  of the parton of the photon entering the hard scattering process shown in Fig. 1b is measured and used to extract the gluon density in leading order in the photon. This analysis follows closely that presented in [6], where the kinematics of the hard scattering process were reconstructed by means of jets measured in the detector. In the analysis presented here the measured variable  $x_\gamma^{rec}$ , which is found to be correlated with the true value of  $x_\gamma$  of the parton entering the scattering, is based on charged tracks with a high transverse momentum  $p_T$ . This method thus avoids two large systematic errors entering in the jet analysis. These are the energy scale uncertainty of the calorimeter and the uncertainty of the jet energy measurement due to overlap with energy deposits from soft multiple interactions which may occur on top of the hard scattering process. The drawback of this method is a stronger sensitivity to fragmentation uncertainties.

---

<sup>1</sup>  $\theta$  is the polar angle of the particle in the HERA laboratory frame, measured with respect to the proton beam direction.

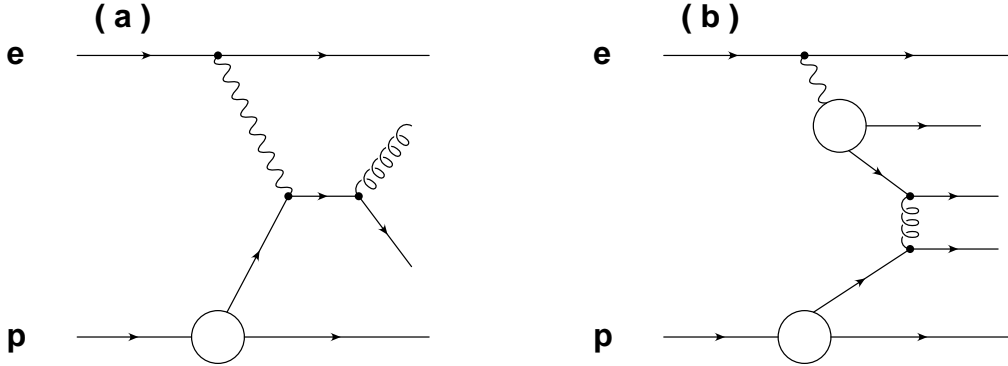


Figure 1: Examples of diagrams for direct (a) and resolved (b) photon processes in  $ep$  scattering; in (b) a gluon has the space-like virtuality of the probe and a quark is resolved in the photon; similarly gluons in the photon can be resolved by quarks and gluons with space-like virtuality.

## 2 The Apparatus

The data were collected with the multi-purpose detector H1 at the HERA collider in 1994, in which electrons<sup>2</sup> of 27.5 GeV collided with protons of 820 GeV. The total data sample corresponds to a luminosity of  $1.35 \pm 0.02 \text{ pb}^{-1}$ .

A detailed description of the H1-detector has been given elsewhere [16]. Here only the components crucial for this particular analysis will be briefly described.

The H1 luminosity system consists of an electron tagger and a photon tagger, located 33 m and 103 m from the interaction point in the electron beam direction, respectively. The luminosity is determined from the rate of Bremsstrahlung process  $ep \rightarrow ep\gamma$  events by detecting the photon. Both detectors are TlCl/TlBr crystal Čerenkov calorimeters with an energy resolution of  $10\%/\sqrt{E(\text{GeV})}$ . The electron detector allows to tag the photoproduction events used in this analysis by detecting electrons scattered at small angles.

The central tracker (CT) consists of inner and outer cylindrical jet chambers,  $z$ -drift chambers and proportional chambers. The two cylindrical drift chambers [17] (CJC), are mounted concentrically around the beamline inside a homogeneous magnetic field of 1.15 Tesla and provide up to 65 space points for a charged track, yielding particle charge and momentum from the track curvature in the polar angular range of  $20^\circ$  and  $160^\circ$ . The transverse momentum resolution is  $\sigma(p_T)/p_T \sim 0.6\% \cdot p_T$  (GeV/c) in the  $p_T$  range  $2 < p_T < 12$  GeV/c considered here. The resolution for the polar angle  $\theta$  is 2 mrad.

The central tracking system is complemented by a forward tracking system. All trackers are surrounded by a fine grained liquid argon sampling calorimeter, consisting of an electromagnetic section with lead absorbers and a hadronic section with steel absorbers.

## 3 Data Analysis

<sup>2</sup>In 1994 the incident lepton at HERA was a positron, but we keep the generic name “electron” for the incident and scattered lepton throughout this paper

### 3.1 Event Selection

Photoproduction events were selected which have the scattered electron detected in the electron tagger, and consequently have a four-momentum transfer  $Q^2 < 10^{-2} \text{ GeV}^2$ , where  $Q^2 = 4E_e E'_e \cos^2(\theta/2)$ . Here  $E_e$  and  $E'_e$  are the incoming and scattered electron energy and  $\theta$  the polar angle of the scattered electron. Tagged events were required to have an electron candidate in the fiducial volume of the electron-tagger with energy  $E'_e > 4 \text{ GeV}$  and to have less than 2 GeV deposited in the photon detector. The latter condition suppresses background from the proton beam, which appears in a random coincidence with the high rate Bethe-Heitler events, and also reduces QED corrections. In addition a track-based trigger was required, which is formed using only 10 selected layers out of 56 radial signal wire layers of the CJC. It demands the presence of at least one track of negative charge with  $p_T > 700 \text{ MeV}/c$  and with a distance of closest approach of less than 2 cm from the nominal beam axis; this requirement suppresses beam-wall background as well as fake tracks from random hits due to synchrotron radiation.

For this analysis the events were required to have  $0.3 < y = E_\gamma/E_e < 0.7$  where  $E_\gamma$  is the photon energy. As a consequence, in the  $\gamma p$  centre-of-mass system (CMS) the energy range is  $165 < \sqrt{s_{\gamma p}} < 251 \text{ GeV}$ , with an average of  $\sqrt{s_{\gamma p}} \sim 200 \text{ GeV}$ . An interaction vertex, reconstructed using tracks in the CT, had to be in the range  $-25 < z_V < +35 \text{ cm}$ , where  $z_V$  is the  $z$  coordinate of the reconstructed vertex.

A total of about 960 000 events satisfy all described criteria. The remaining non- $ep$  background was determined by analysing data from electron pilot bunches (i.e. electron bunches which have no colliding proton bunch partner) and from a monitoring trigger of minimum bias events. It was found to be less than 2.7% at this stage of selection, before tighter cuts on track quality and transverse momentum were applied.

### 3.2 Track Selection

For this analysis tracks from the central tracker were selected which have a transverse momentum with respect to the beam axis of at least 2 GeV/c, a pseudorapidity measured in the HERA laboratory reference system of  $|\eta| < 1$  and a minimum track length  $\Delta R$  of 30 cm in the  $x - y$  plane. The latter cut is essential to ensure a good measurement of  $p_T$  of the track, from 2 up to 12 GeV/c, which is the range considered here. To minimize the systematic errors, sectors of the CT in  $\phi$ , the azimuthal angle, which had a lower efficiency have been excluded from the analysis. A total of 16591 tracks was selected for the analysis, resulting from 15543 events.

### 3.3 Corrections and Background

The residual background from beam-gas, beam-wall, and pile-up events, after demanding a well-measured, high  $p_T$  track such as defined above, was found to be negligible. The background from cosmic events was removed by rejecting events with two oppositely charged tracks meeting the requirements above (except for  $\phi$  region cut), and which were aligned in  $\theta$  and  $\phi$  to better than  $5^\circ$ . All events rejected by this cut were visually checked and confirmed to be cosmic events, and all were found to have at least one track with  $p_T > 6 \text{ GeV}/c$ . Conversely, all events with at least one track with  $p_T > 6 \text{ GeV}/c$  were visually scanned but no further cosmic event was found. A check for the potential contamination from DIS overlap events was also performed: no such events were found.

In order to obtain the produced number of tracks,  $N_{tr}$ , the observed number of events and tracks were corrected as follows:

- $A_{etag}$ : The geometrical acceptance of the electron tagger, determined as described in [18], was corrected as a function of  $y$ . On average the acceptance is 55% for  $0.3 < y < 0.7$ . The tagger efficiency within the chosen acceptance is 100%.
- $\epsilon_{trig}$ : The CJC trigger efficiency has been estimated by comparing the detection rates for samples of events with the main trigger and a minimum bias trigger for  $e$ -tagged events. For the high  $p_T$  range considered here, it was estimated to be  $96.3 \pm 1.2\%$ , independent of  $p_T$ ,  $\eta$  and  $\phi$ .
- $\epsilon_{track}$ : The overall track efficiency contains three multiplicative factors: (i) The efficiency for finding and reconstructing single tracks,  $\epsilon_{rec}$ , was taken from Monte Carlo studies and found to be  $99.2 \pm 0.8\%$ . The agreement between data and Monte Carlo was verified by visual scanning of events in both samples. (ii) The efficiency of the cut on transverse track length,  $\epsilon_{\Delta R}$ , was estimated from data to be  $97.9 \pm 0.4\%$ . This was checked to be independent of both  $\eta$  and  $\phi$ . (iii) The  $\phi$ -restriction,  $\epsilon_\phi$ , of the geometrical acceptance of the central drift chamber was accounted for assuming a uniform distribution in  $\phi$ , and amounts to 53.1%.
- The bin-to-bin migration in  $p_T$ ,  $\epsilon_{mig}$ , due to the rapidly decreasing  $p_T$  spectrum and to the finite resolution in  $p_T$ , was estimated from a Monte Carlo simulation and for the varying bin sizes used here it was found to be a simple multiplicative factor  $103.8 \pm 1.3\%$ , independent of  $p_T$ .

The total correction factor for tracks is then  $51.5 \pm 2.0\%$ , where the systematic errors have been added in quadrature. The uncertainties on these correction factors, were taken as systematic errors. Detailed checks and comparisons with Monte Carlo led to the introduction of an extra systematic error, to account for a remaining uncertainty in the  $p_T$  measurement, which showed up in two ways: in the ratio of positively and negatively charged tracks and in the efficiency determination for a stronger cut on the transverse track length ( $\Delta R > 50$  cm). The resulting uncertainty was parameterized as  $2\% \cdot p_T / (\text{GeV}/c)$  at the centre of each bin for  $p_T$  distributions, and as  $2\% \cdot p_T^{low} / (\text{GeV}/c)$  for  $\eta$  distributions, with  $p_T^{low}$  the lowest  $p_T$  value of particles included in the distribution.

All systematic uncertainties were added in quadrature, except for the overall uncertainty of 5% from the luminosity measurement and the electron tagger acceptance which is not included in the error bars shown in the figures below.

## 4 Monte Carlo Simulation Programs

The PYTHIA 5.7 event generator [19] was used to simulate photon-proton interactions. As well as the leading order cross-section, PYTHIA includes initial- and final-state QCD parton radiation effects which are calculated in the leading logarithmic approximation. The strong coupling constant  $\alpha_s$  was calculated in first order QCD using  $\Lambda_{\text{QCD}} = 200$  MeV for 4 quark flavours. For the parton distributions of the proton the GRV-LO [20] set was used.

The model calculations were made for different sets of the parton densities in the photon: GRV [21], SAS1D [22] and LAC1 [23]. All these parametrizations were extracted from QCD fits to photon structure function data measured in  $e\gamma$  collisions from  $e^+e^-$  interactions, but have different assumptions for the gluon content, which is only weakly constrained by these measurements. In particular LAC1 assumes a large gluon content of the photon at small- $x$  values which is larger than for both other parametrizations. The GRV and SAS1D distributions both start the evolution from a small starting scale,  $Q_0^2 = 0.25$  GeV<sup>2</sup> and 0.36 GeV<sup>2</sup> respectively,



a procedure which has turned out to be quite successful for the parton densities in the proton. The different treatment of the vector meson valence quark distributions leads to a larger gluon component at small- $x$  of the photon for the GRV compared to the SAS1D parton densities.

Multiple parton interactions were generated in addition to the primary parton–parton scattering. They are calculated as leading order QCD processes between partons from the photon and proton remnants. The transverse momentum of all (primary and multiple) parton–parton interactions was required to be above a cut-off value of  $p_T^{min}$ , depending on the photon structure function. For the parton densities used here the values  $p_T^{min} = 1.2, 1.0$  and  $2.0$  GeV/c have been used for GRV, SAS1D and LAC1 respectively. These values have been found to give an optimal description of the transverse energy flow outside jets [7].

The PHOJET 1.06 event generator [24], based on the two-component Dual Parton model [25] has been used as well. PHOJET incorporates very detailed simulations of both multiple soft and hard parton interactions on the basis of a unitarization scheme. It also includes initial- and final-state interactions. For the distributions shown below, it was verified that the PYTHIA and PHOJET predictions for the GRV parton distributions for the proton and the photon agree to better than 5%.

Hadronization in both PHOJET and PYTHIA was modelled with the LUND string fragmentation scheme (JETSET 7.4 [26]). Since the kinematics of the hard scattering process will be related to the  $p_T$  values of the particles with high transverse momentum, it is imperative to study the fragmentation dependence of this measurement. A model with a different hadronization scheme, HERWIG [27], was used for this purpose. In this model the hadronization is based on cluster fragmentation. Other parameters, such as the parton densities for the photon and proton, were taken to be the same as for PYTHIA. Both the LUND model and HERWIG were found to give a good description of the general features of fragmentation as measured in  $e^+e^-$  collisions at LEP (e.g. [28]).

## 5 Inclusive Charged Particle Cross Sections

The invariant cross-section for single particle production is given by

$$\frac{d^2\sigma}{dp_T^2 d\eta} = \int \frac{d^3\sigma}{dp_T^2 d\eta d\phi} \cdot d\phi = \pi \cdot E \cdot \frac{d^3\sigma}{dp^3} \quad (1)$$

assuming azimuthal symmetry of the cross-section allowing integration over  $\phi$ . The measurement was made at a  $\sqrt{s_{\gamma p}} \sim 200$  GeV, and effectively averages over the region  $165 \text{ GeV} < \sqrt{s_{\gamma p}} < 251 \text{ GeV}$ . No significant  $\sqrt{s_{\gamma p}}$  dependence was found when the data were subdivided in two  $\sqrt{s_{\gamma p}}$  bins. The cross-section for inclusive charged particle production in  $\gamma p$  collisions was calculated from the corrected number of tracks produced,  $N_{tr}$ , in a bin of  $p_T$  and  $\eta$ . It is given by:

$$\frac{d^2\sigma_{\gamma p}}{dp_T^2 d\eta} = \frac{N_{tr}(p_T, \eta)}{\mathcal{L} \cdot F \cdot 2p_T \Delta p_T \cdot \Delta \eta} \quad (2)$$

where  $\mathcal{L}$  denotes the integrated luminosity,  $F$  is the photon flux integral and the flux  $f(y)$  is defined according to  $d\sigma(ep) = \sigma(\gamma p) \cdot f(y) \cdot dy$ . For the chosen  $y$ -range the integral over  $y$  of the photon flux yields  $F = 0.0136$ , assuming the Weizsäcker-Williams approximation [29, 30].  $\Delta\eta$  and  $\Delta p_T^2 = 2 \cdot p_T \cdot \Delta p_T$  are the bin widths.

The resulting differential cross-section for the sum of positive and negative charged particles is shown in Fig. 2a. The error bars denote the statistical and systematic errors added in quadrature. The measured cross-sections are listed in Table 1. The data exhibit a strong improvement in

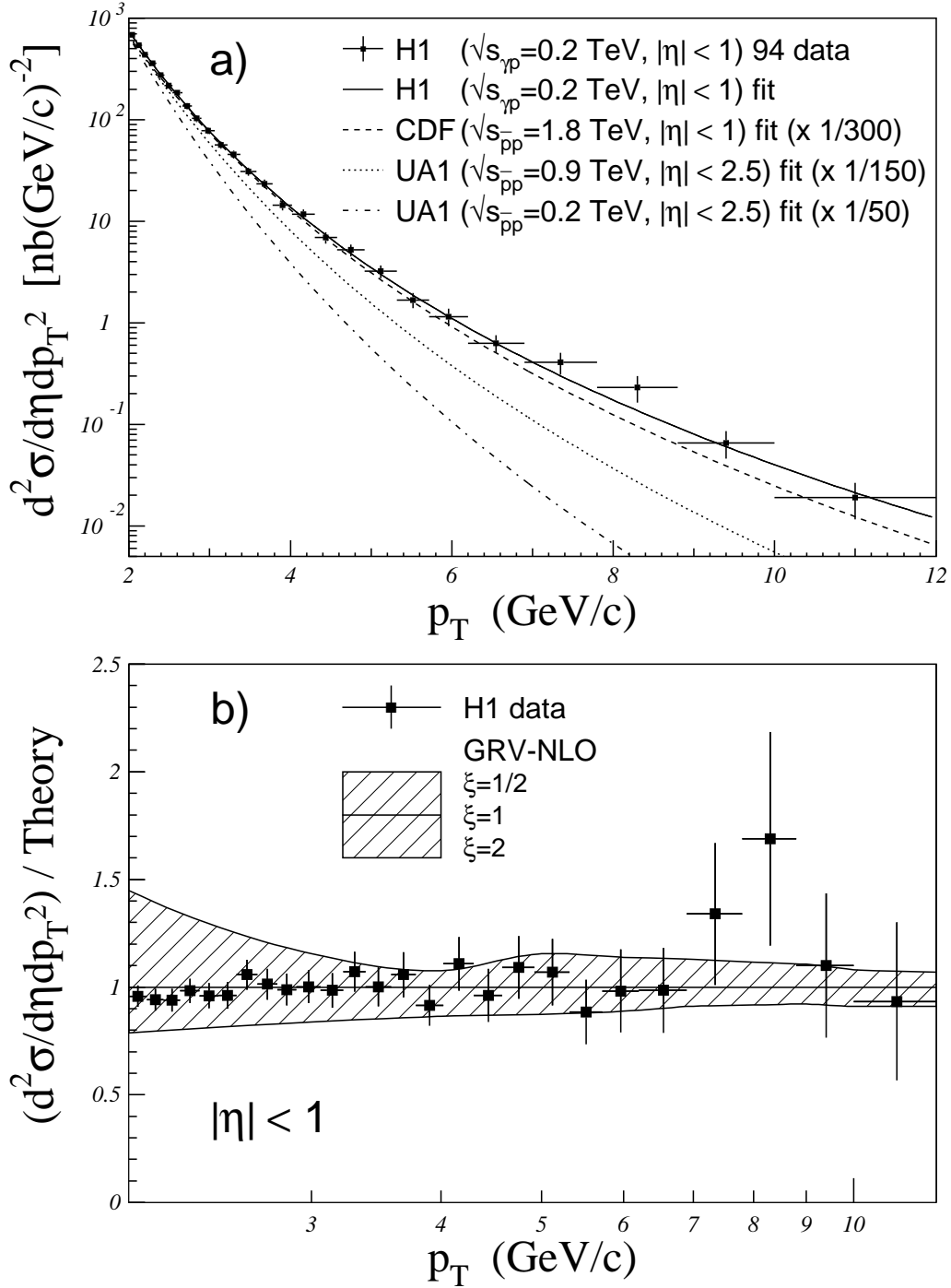


Figure 2: **a)** The inclusive  $\gamma p$  cross-section for charged particles in photoproduction (full squares) measured in the kinematical region  $|\eta| < 1.0$  at an average  $\sqrt{s_{\gamma p}} \approx 200$  GeV. The error bars denote the statistical and systematic errors added in quadrature. An overall uncertainty of 5% from the luminosity measurement and the electron tagger acceptance is not included in the errors. The curves indicate power-law fits, as described in the text, for these data and for the  $p\bar{p}$  data from UA1 and CDF as given in [32, 33]. **b)** The ratio of data over the NLO QCD calculation with scale  $\xi p_T^2$  for  $\xi = 1$ . The shaded band shows the expected variation of the ratio as  $\xi$  changes from 0.5 to 2, illustrating the sensitivity of the QCD calculation to the renormalization and factorization scales (see text).

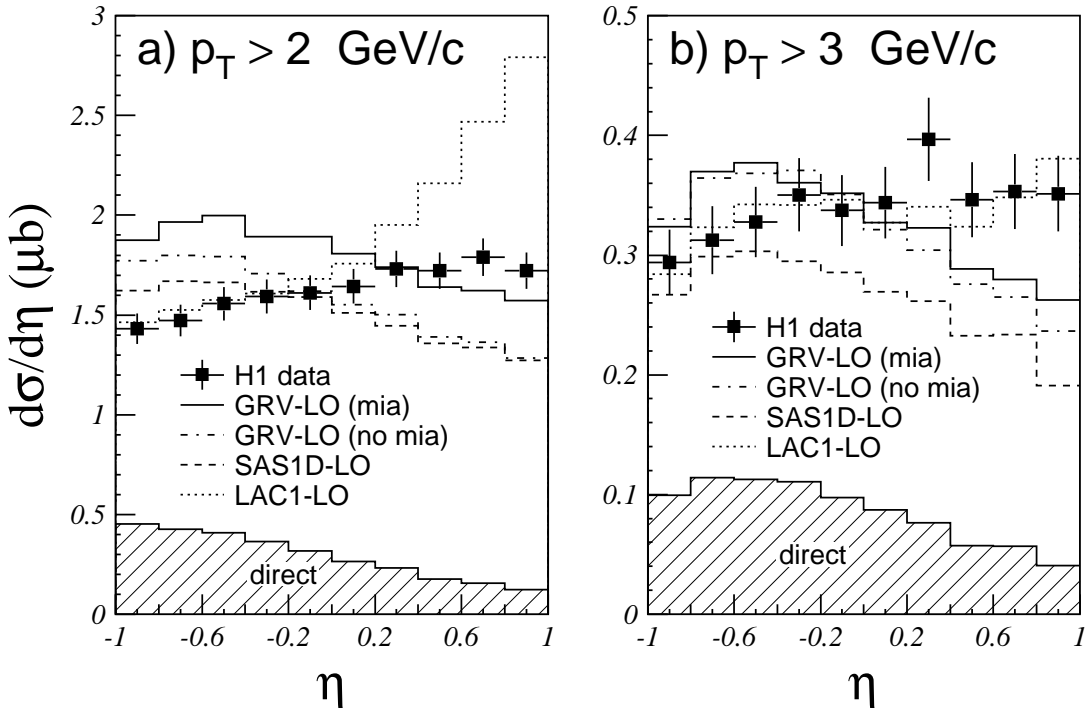


Figure 3: The differential  $\gamma p$  cross-section  $d\sigma/d\eta$  for inclusive production of high  $p_T$  charged particles (full squares) in comparison with LO QCD calculation by PYTHIA (histograms). The error bars denote the statistical and systematic errors added in quadrature. An overall uncertainty of 5% from the luminosity measurement and electron tagger acceptance is not included. Different lines represent different photon structure function parametrizations: GRV with (full) and without (dash-dotted) multiple interactions, SAS1D (dashed) and LAC1 (dotted). The contributions from the direct photon processes are shown as shaded histograms.

precision compared to the previous H1 measurement [5] and cross-sections are now given up to 12 GeV/c in  $p_T$ . The QCD inspired power-law [31] expression

$$E \cdot \frac{d^3\sigma}{dp^3} = A \cdot \left(1 + \frac{p_T}{(p_T)_0}\right)^{-n}. \quad (3)$$

was fitted to the data. The fitted curve is shown in Fig. 2a, and describes the data well over the whole  $p_T$  range. The fit gives  $A = 5.44 \pm 0.66$  mb and  $n = 7.03 \pm 0.07$  (statistical errors). The parameter  $(p_T)_0$  was fixed to the value 0.63, as found in [5], but other values in the range 0.5–0.75 were found to give equally good fits. The effect of the choice of  $(p_T)_0$  leads to an uncertainty in the power  $n$  of about 0.2.

Also shown in Fig. 2a are the results of similar fits to the  $p\bar{p}$  collider data of the UA1-collaboration [32] in the rapidity region  $|\eta| < 2.5$ , at CMS energies  $\sqrt{s} = 200$  and 900 GeV, and of CDF [33] in the rapidity region  $|\eta| < 1$ , at  $\sqrt{s} = 1800$  GeV, scaled by the factors indicated in the figure, which essentially normalizes all data to the  $\gamma p$  cross-section at  $p_T = 2$  GeV/c. The high  $p_T$  tail is observed to increase with increasing energy in  $p\bar{p}$ . The hardness of the  $\gamma p$  spectrum is comparable to that of the  $p\bar{p}$  data at the highest energy. The high  $p_T$  tail in the data is clearly larger than in  $p\bar{p}$  collisions at similar CMS energy, which can be understood as being due to extra contributions in  $\gamma p$ , namely the direct and the pointlike resolved (or anomalous) component [5].

In Fig. 2b the ratio of data to the NLO calculation [34] using GRV structure functions for photon and proton is shown. Both renormalization and factorization scales were chosen to be

$p_T$ [GeV/c]	$\frac{d\sigma^{\gamma p}}{dp_T^2 d\eta}$ (nb/(GeV/c) <sup>2</sup> )	$\Delta \frac{d\sigma^{\gamma p}}{dp_T^2 d\eta}$ (nb/(GeV/c) <sup>2</sup> )
2.00 – 2.08	685.0	35.2
2.08 – 2.16	539.1	29.3
2.16 – 2.24	434.2	24.7
2.24 – 2.34	359.9	20.7
2.34 – 2.44	274.3	16.7
2.44 – 2.54	216.6	13.9
2.54 – 2.66	184.8	12.1
2.66 – 2.78	135.9	9.53
2.78 – 2.90	102.8	7.64
2.90 – 3.06	78.32	5.97
3.06 – 3.22	56.41	4.59
3.22 – 3.38	45.62	3.97
3.38 – 3.58	31.01	2.82
3.58 – 3.78	23.47	2.32
3.78 – 4.02	14.33	1.49
4.02 – 4.30	11.79	1.33
4.30 – 4.58	6.905	0.885
4.58 – 4.92	5.210	0.692
4.92 – 5.32	3.224	0.465
5.32 – 5.72	1.673	0.283
5.72 – 6.20	1.148	0.225
6.20 – 6.90	0.631	0.126
6.90 – 7.80	0.408	0.100
7.80 – 8.80	0.232	0.068
8.80 – 10.0	0.066	0.020
10.0 – 12.0	0.019	0.007

Table 1: Measured differential cross-section and total errors ( $\Delta$ ) for the production of charged particles in the  $\eta$  range  $-1$  to  $1$ . An overall uncertainty of 5% from the luminosity and electron tagger acceptance is not included.

$\eta$	$p_T > 2.0$ GeV/c		$p_T > 3.0$ GeV/c	
	$\frac{d\sigma}{d\eta}$ (nb)	$\Delta \frac{d\sigma}{d\eta}$ (nb)	$\frac{d\sigma}{d\eta}$ (nb)	$\Delta \frac{d\sigma}{d\eta}$ (nb)
-1.0 – -0.8	1431.1	77.8	293.9	27.2
-0.8 – -0.6	1473.1	79.4	312.3	28.4
-0.6 – -0.4	1556.3	83.2	327.6	29.3
-0.4 – -0.2	1593.3	85.1	350.3	30.7
-0.2 – -0.0	1611.9	85.3	337.4	29.6
0.0 – 0.2	1643.8	87.5	343.7	29.8
0.2 – 0.4	1730.2	91.2	396.8	34.8
0.4 – 0.6	1721.3	90.9	346.1	31.4
0.6 – 0.8	1790.4	94.0	353.3	31.3
0.8 – 1.0	1721.2	90.6	351.4	31.5

Table 2: Measured differential cross-section and total errors ( $\Delta$ ) for the production of charged particles. An overall uncertainty of 5% from the luminosity and electron tagger acceptance is not included.

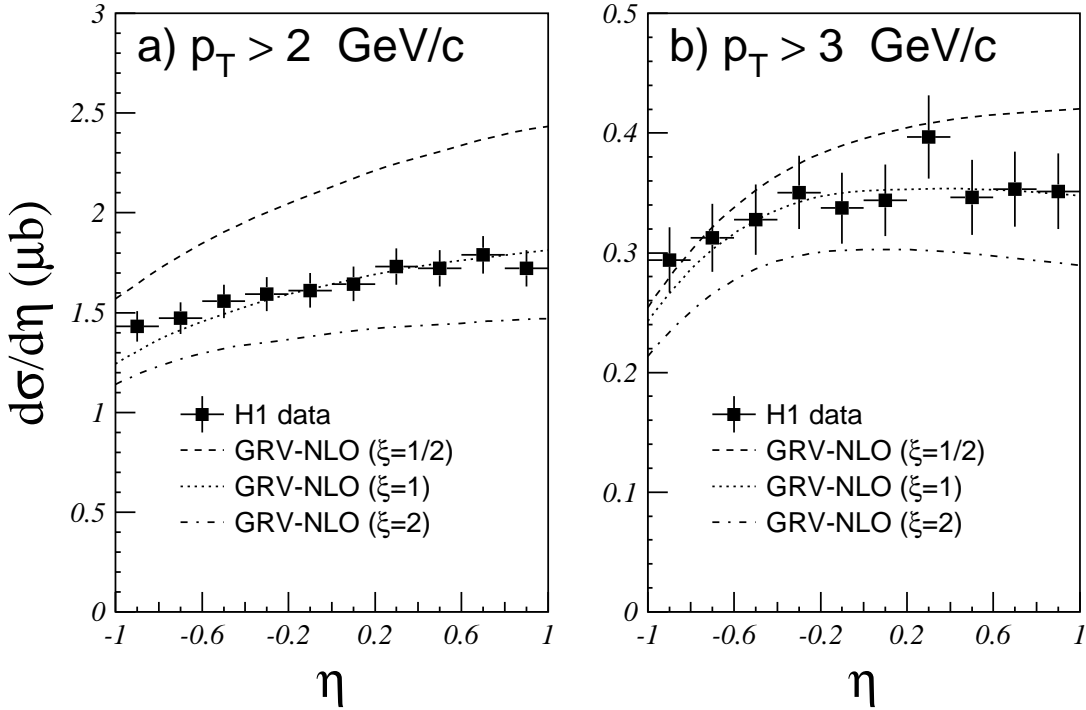


Figure 4: The differential  $\gamma p$  cross-section  $d\sigma/d\eta$  for inclusive production of the high  $p_T$  charged particles (full squares) in comparison with NLO QCD calculations [34], with different values of the scale, taken as  $\mu = \xi p_T^2$ . The error bars denote the statistical and systematic errors added in quadrature. An overall uncertainty of 5% from the luminosity measurement and electron tagger acceptance is not included.

$p_T^2$ . The effect of this choice is shown by predictions for a scale of  $\xi p_T^2$ , with  $\xi = 0.5$  and 2, shown as a ratio to the prediction for  $\xi = 1$ . The calculations describe the data well, in particular when  $\xi$  is close to one.

The dependence of the cross-section on the pseudorapidity  $\eta$ ,  $d\sigma/d\eta$ , is shown in Fig. 3 for all particles with  $p_T$  larger than 2 and 3 GeV/c. The measured cross-sections are listed in Table 2. Note, that the  $\eta$  measured in the HERA laboratory frame is on average shifted by +2 units with respect to the  $\eta^*$  distribution in the  $\gamma p$  CMS system. The spread of this shift due to the photon energy range is less than 0.3 units in pseudorapidity. Therefore the  $\eta$  and  $\eta^*$  distributions look very similar. The data are consistent with being flat in most of the region, with a slight decrease towards  $\eta = -1$ , i.e. in the photon direction. The data are compared with predictions of LO QCD calculations made with PYTHIA, for different structure functions of the photon and assumptions on the soft interactions in the underlying event (cf. section 4). Predictions are shown for GRV with (full) and without (dash-dotted) multiple interactions, SAS1D (dashed) and LAC1 (dotted). For the latter two predictions multiple interactions were included. All structure functions except LAC1 show a falling distribution with increasing  $\eta$ , contrary to the data. The contributions from the direct photon processes are shown as shaded histogram and decrease towards the proton direction. For the data with  $p_T > 2$  GeV/c, there is a strong sensitivity to the parton distributions in the photon, and also to the amount of underlying interactions as shown by the GRV curves. None of the predictions presented shows satisfactory agreement with the data. For data with  $p_T > 3$  GeV/c, the effect of multiple interactions becomes very small, as shown for the GRV predictions. The sensitivity to the photon structure is also reduced but is still significant. For large  $p_T$  the data agree best with LAC1, and disagree with SAS1D. It was checked that these results do not depend on the choice of the parton distributions of the proton,

when selected from those consistent with the most recent proton structure function data.

In Fig. 4 the cross-sections as a function of  $\eta$  are compared with NLO calculations, including direct and resolved contributions. The NLO calculations [34] reproduce the data, however one can see a significant effect of the choice of the QCD scale on both the shape and normalization of the distributions, as shown by the curves for different  $\xi$  values. The effect is smaller for data with  $p_T > 3$  GeV/c. The scale has also been found to be the reason for the considerable difference between the LO and NLO GRV cross-section predictions. PYTHIA uses as a scale the  $p_T$  of the hard partonic interaction, while the program of [34] uses the  $p_T$  of the final state particle, which can differ substantially from that of the original parton.

## 6 The $x_\gamma$ Distribution and Gluon Density in the Photon

In this section the distribution of the momentum fraction  $x_\gamma = E_{parton}/E_\gamma$  of the parton of the photon entering the hard scattering process will be determined from the charged tracks. For this analysis events were kept which have at least one track reconstructed with a  $p_T > 2.6$  GeV/c. This value is a compromise between large systematic uncertainties from multiple interactions and the statistical precision. In total 9378 events have been selected.

For each event with at least one measured track of a charged particle with  $p_T > 2.6$  GeV/c the variable  $x_\gamma^{rec}$  was calculated:

$$x_\gamma^{rec} = \frac{\sum p_T e^{-\eta}}{E_\gamma} \quad (4)$$

where the sum runs over all tracks with  $p_T > 2$  GeV/c. This variable is correlated to the true  $x_\gamma$  of the interaction. Apart from the strongly reduced sensitivity to effects of multiple interactions, the requirement  $p_T > 2.6$  GeV/c ensures that the data stay safely away from the region which is affected by the  $p_T^{min}$  cut used in the Monte Carlo event generation (cf. section 4).

Monte Carlo events were used to study the correlation between the measured  $x_\gamma^{rec}$  and the true  $x_\gamma$ , shown in Fig. 5. The generated events were fed into the detailed H1 simulation program and then subjected to the same reconstruction and analysis chain as the real data. The correlation is shown for the Monte Carlo events generated with the PYTHIA program, using the LAC1 parametrization of the structure function of the photon.

For the reconstruction of the true  $x_\gamma$  an unfolding procedure was used [35], following the analysis as detailed in [6]. Monte Carlo events generated with PYTHIA using the LAC1 parton densities have been used for the unfolding. The result is presented in three bins in  $x_\gamma$ , a condition imposed by the unfolding procedure, in order to minimize the bin-to-bin correlations. The resulting  $x_\gamma$  distribution is shown in Fig. 6, with statistical errors only, which include the bin-to-bin correlations from the unfolding. The dotted curve is the prediction of the PYTHIA model with the LAC1 parton distributions for the photon. The dashed curve shows the component of the event rate where only quarks from the photon side are involved. The quark distribution in the photon is rather well constrained from  $e\gamma$  measurements as discussed in section 1 above. The full calculation gives a fair description of the measurement, and a large contribution of gluon induced processes (from the photon side) [6] is clearly confirmed.

The gluon distribution in the photon, extracted at leading order, was then obtained from the  $x_\gamma$  distribution as follows. The contribution of processes in which quarks are resolved in the photon (for example Fig. 1(b)) were calculated and subtracted from the data. The ratio of the subtracted data distribution with the distribution calculated from Monte Carlo using only processes initiated by a gluon from the photon side gives weight factors. Applying these

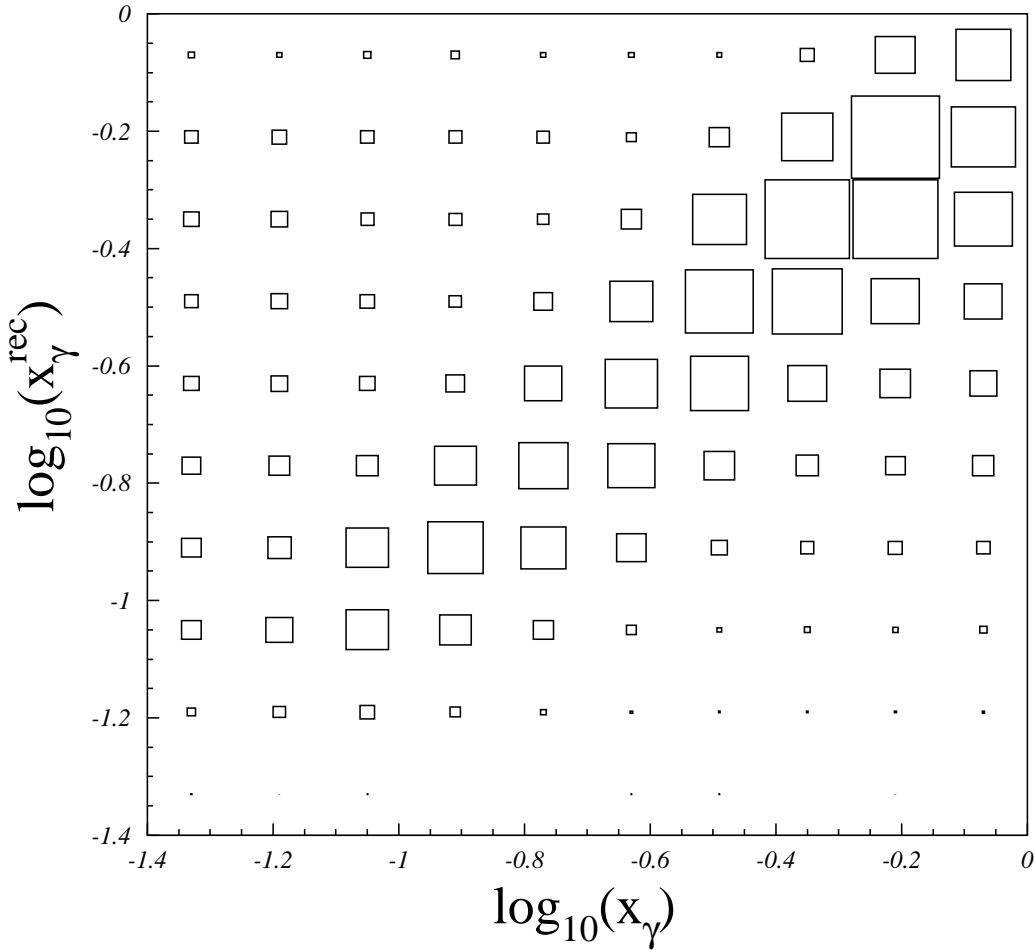


Figure 5: Correlation between reconstructed and true  $x_\gamma$  values using the PYTHIA Monte Carlo with the LAC1 parton densities for the photon.

weight factors to the input gluon distribution used in the Monte Carlo yields the measured gluon distribution, which is shown in Fig. 7. The average transverse momentum squared of the hard partonic scattering for this data sample amounts to  $\langle p_T^2 \rangle = 38 \text{ GeV}^2/c^2$ , as derived from Monte Carlo studies, and is taken as the scale for comparisons with parton densities. The total errors include statistical and systematic errors where all contributions have been added in quadrature. Apart from the systematic errors already included in the cross-section measurements discussed previously, the following systematic errors specific to the unfolding had to be taken into account:

- The uncertainty in the quark density of the photon was found to be 15% by repeating the analysis with different parametrizations of the quark distributions [21, 22, 23].
- A variation of the unfolding parameters led to a 10% uncertainty.
- Changes of up to 20% were observed when different fragmentation models (PYTHIA, PHOJET, HERWIG) and different parton densities for the photon structure (GRV, LAC1) were selected in the Monte Carlo used for the unfolding. Hence a 20% systematic error from this source was assumed.

The uncertainty in the parton densities of the proton is negligible compared to the uncertainties above and this was neglected.

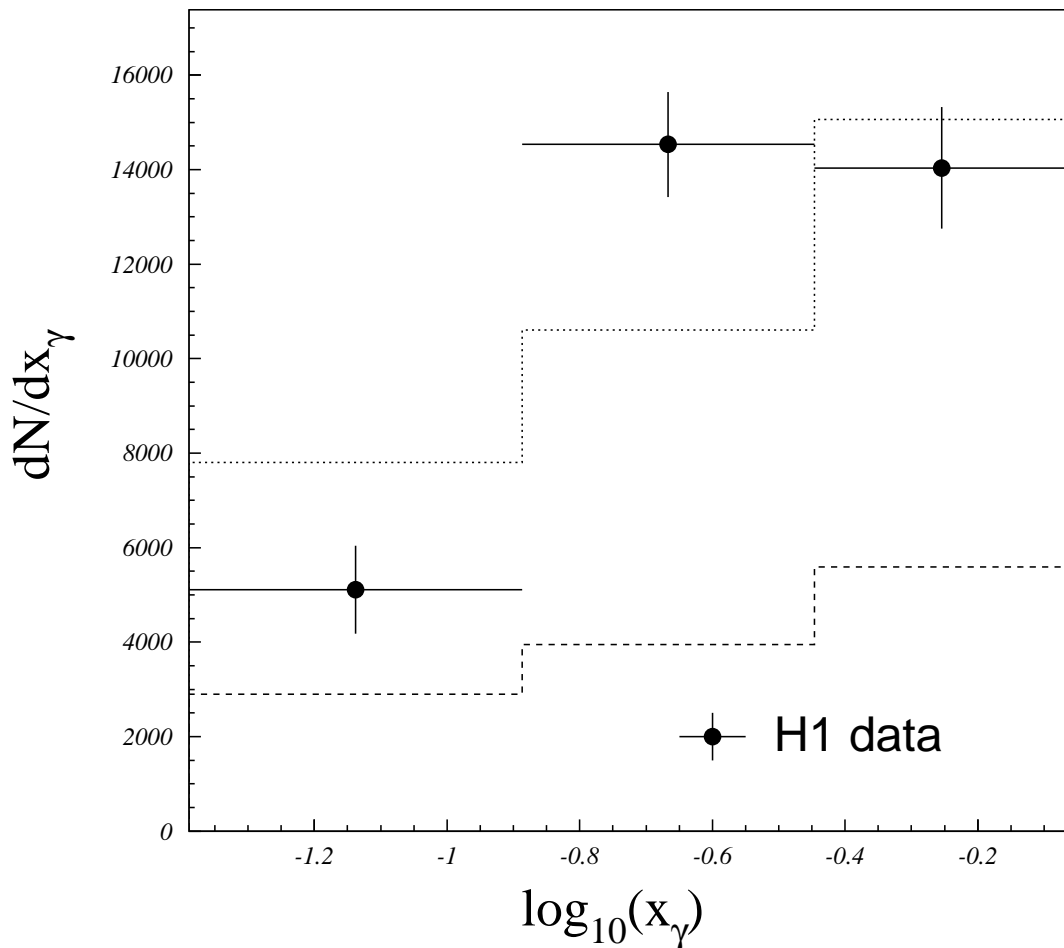


Figure 6: The  $x_\gamma$  distribution in the photon. The errors are statistical only. The curves are full (dotted line) and ‘quark only’ (dashed line) predictions of PYTHIA, using the LAC1 parton distributions of the photon.

The result is compared with the measurements based on the 1993 H1 data [6], using jets instead of charged tracks. The average transverse momentum squared of the hard partonic scattering for the jet data sample amounts to  $\langle p_T^2 \rangle = 75 \text{ GeV}^2/c^2$ . The measurements are found to be consistent. The improvement in precision of the measurement presented here is clearly visible. The results confirm that the contribution of the gluon to photon structure is significant. The gluon density tends to rise with decreasing  $x_\gamma$ . The result is compared with various parton distributions: LAC1, GRV, SAS1D. They are generally in agreement with the data.

## 7 Conclusions

The differential cross-sections  $d\sigma/dp_T^2$ , for  $|\eta| < 1$  in the HERA laboratory frame, and  $d\sigma/d\eta$  for  $p_T > 2 \text{ GeV}/c$  and  $p_T > 3 \text{ GeV}/c$  have been measured in photoproduction events with the H1 detector. The  $p_T$  spectrum exhibits a high  $p_T$  tail, larger than in  $p\bar{p}$  collisions at similar centre of mass energy. The  $\eta$  spectra show sensitivity to the parton densities in the photon. When charged particles down to  $p_T = 2 \text{ GeV}/c$  are included, there is also a significant effect from the activity in the underlying event. Charged tracks have been used to extract information



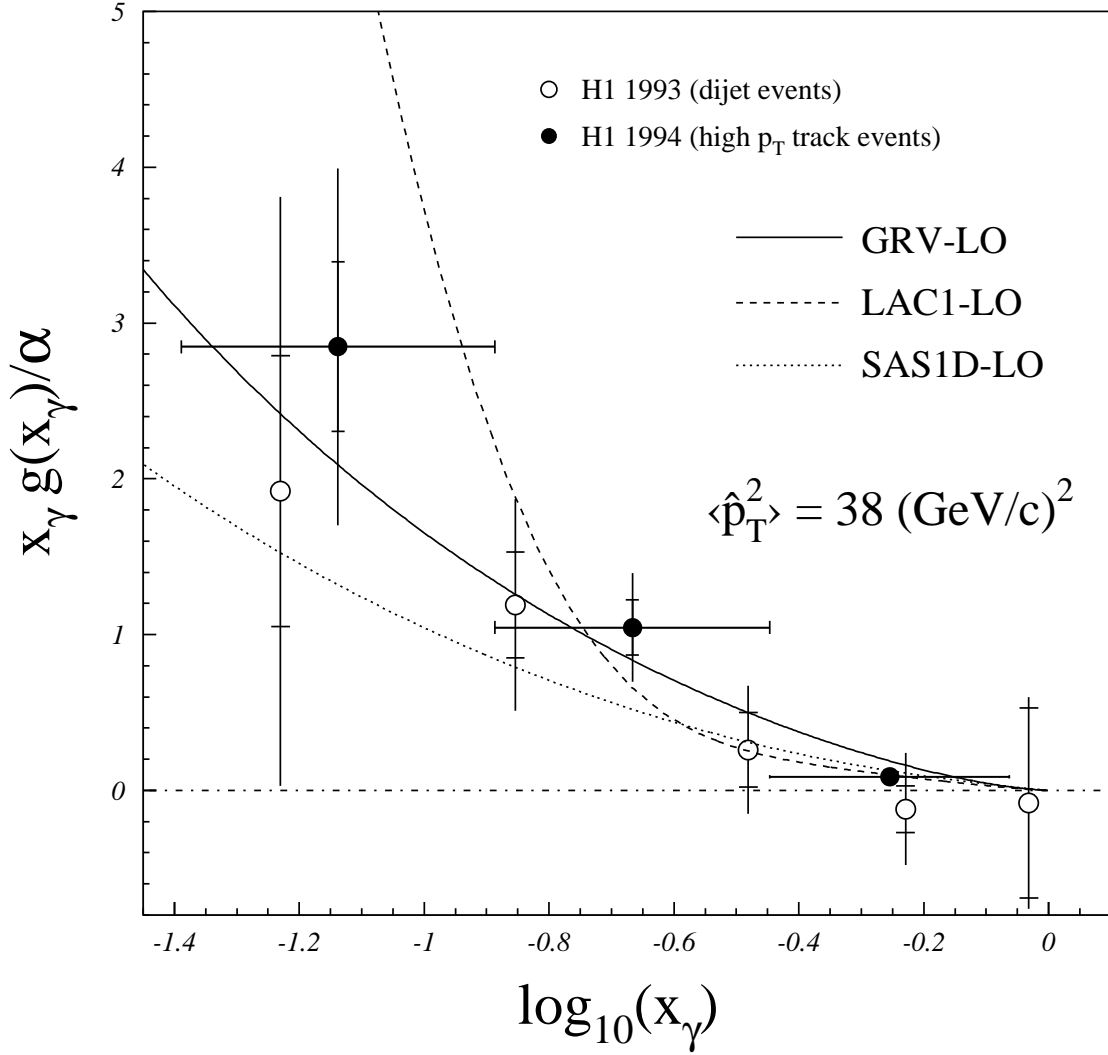


Figure 7: The LO gluon distribution in the photon from charged tracks (full circles;  $\langle p_T^2 \rangle = 38 \text{ GeV}^2/c^2$ ) and jets (open circles;  $\langle p_T^2 \rangle = 75 \text{ GeV}^2/c^2$ ). The inner error bars are statistical, the full bars are the statistical and systematic errors added in quadrature. An overall uncertainty of 5% from the luminosity measurement and the electron tagger acceptance is not included in the errors. The curves are GRV [21] (full line), SAS1D [22] (dotted line) and LAC1 [23] (dashed line).

on the hadronic structure of the photon, by measuring the  $x_\gamma$  distribution. The  $x_\gamma$  distribution has been unfolded from the data using for the first time high  $p_T$  charged tracks to extract the LO gluon density of the photon. The gluon density is found to increase with decreasing  $x_\gamma$  in agreement with an earlier H1 analysis using jets to tag and reconstruct the hard sub-process.

## Acknowledgements

We are grateful to the HERA machine group whose outstanding efforts have made and continue to make this experiment possible. We thank the engineers and technicians for their work in constructing and now maintaining the H1 detector, our funding agencies for financial support, the DESY technical staff for continual assistance, and the DESY directorate for the hospitality which they extend to the non-DESY members of the collaboration. We have benefited from a number of helpful discussions with B.A. Kniehl.

## References

- [1] J. J. Sakurai, *Ann. Phys.* 11 (1960) 1;  
M. Gell-Mann and F. Zachariasen, *Phys. Rev.* 124 (1961) 953.
- [2] PLUTO Collab., Ch. Berger et al., *Nucl. Phys.* B281 (1987) 365.  
JADE Collab., W. Bartel et al., *Z. Phys.* C24 (1984) 231.  
TASSO Collab., M. Althoff et al., *Z. Phys.* C31 (1986) 527.  
TPC/2 $\gamma$  Collab., H. Aihara et al., *Z. Phys.* C34 (1987) 1.  
AMY Collab., S.K. Sahu et al., *Phys. Lett.* B346 (1995) 208.  
TOPAZ Collab., K. Muramatsu et al., *Phys. Lett.* B332 (1994) 477.  
DELPHI Collab., P. Abreu et al., *Z. Phys.* C69 (1996) 223.  
OPAL Collab., K. Ackerstaff et al., *Z. Phys.* C74 (1997) 33.
- [3] H1 Collab., I. Abt et al., *Phys. Lett.* B297 (1992) 205.
- [4] H1 Collab., I. Abt et al., *Phys. Lett.* B314 (1993) 436.
- [5] H1 Collab., I. Abt et al., *Phys. Lett.* B328 (1994) 176.
- [6] H1 Collab., T. Ahmed et al., *Nucl. Phys.* B445 (1995) 195.
- [7] H1 Collab., S. Aid et al., *Z. Phys.* C70 (1996) 17.
- [8] H1 Collab., C. Adloff et al., *Eur. Phys. J. C*1 (1998) 97.
- [9] ZEUS Collab., M. Derrick et al., *Phys. Lett.* B297 (1992) 404.
- [10] ZEUS Collab., M. Derrick et al., *Phys. Lett.* B322 (1994) 287.
- [11] ZEUS Collab., M. Derrick et al., *Phys. Lett.* B342 (1995) 417.
- [12] ZEUS Collab., M. Derrick et al., *Phys. Lett.* B348 (1995) 665.
- [13] ZEUS Collab., M. Derrick et al., *Z. Phys.* C67 (1995) 227.
- [14] ZEUS Collab., M. Derrick et al., *Phys. Lett.* B384 (1996) 401.
- [15] ZEUS Collab., J. Breitweg et al., *Eur. Phys. J. C*1 (1998) 109.
- [16] H1 Collab., I. Abt et al., *Nucl. Instr. and Methods* A386 (1997) 310.  
H1 Collab., I. Abt et al., *Nucl. Instr. and Methods* A386 (1997) 348.
- [17] J. Bürger et al., *Nucl. Instr. and Methods* A279 (1989) 217.
- [18] H1 Collab., S. Aid et al., *Z. Phys.* C69 (1995) 27.

- [19] T. Sjöstrand, CERN-TH-6488 (1992), *Comp. Phys. Commun.* 82 (1994) 74.
- [20] M. Glück, E. Reya and A. Vogt, *Z. Phys.* C53 (1992) 127.
- [21] M. Glück, E. Reya and A. Vogt, *Phys. Rev.* D46 (1992) 1973.
- [22] G. A. Schuler, T. Sjostrand, *Phys. Lett.* B376 (1996) 193.
- [23] H. Abramowicz, K. Charchula, A. Levy, *Phys. Lett.* B269 (1991) 458.
- [24] R. Engel, *Z. Phys.* C66 (1995) 203.  
R. Engel and J. Ranft, *Phys. Rev.* D54 (1996) 4244.
- [25] A. Capella et al., *Phys. Rep.* 236 (1994) 225.
- [26] T. Sjöstrand, M. Bengtsson, *Comp. Phys. Commun.* 43 (1987) 367.
- [27] G. Marchesini et al., *Comp. Phys. Comm.* 67 (1992) 465.
- [28] R. Barate et al., ALEPH Collab., *Physics Reports* 294 (1998) 1.
- [29] C. F. Weizsäcker, *Z. Phys.* 88 (1934) 612; E. J. Williams, *Phys. Rev.* 45 (1934) 729.
- [30] S. Frixione, M. L. Mangano, P. Nason, G. Ridolfi, *Phys. Lett.* B319 (1993) 339.
- [31] R. Hagedorn, *Riv. Nuovo Cim.* 6 (1983) 1.
- [32] UA1 Collab., C. Albajar et al., *Nuc. Phys. B* 335 (1990) 261.
- [33] CDF Collab., F. Abe et al., *Phys. Rev. Lett.* 77 (1996) 438.
- [34] F. M. Borzumati, B. A. Kniehl and G. Kramer, *Z. Phys. C* 59 (1993) 341;  
B. A. Kniehl and G. Kramer, *Z. Phys.* C62 (1994) 53;  
B. A. Kniehl, hep-ph/9709261 and Proceedings of the Ringberg Workshop “New Trends in HERA Physics”, Ringberg Castle, Germany, 25-30 May 1997.
- [35] V. Blobel, DESY 84-118 and Proceedings of the CERN School of Computing, Aiguablava (Spain) CERN 1985.